Bandpass Negative Group Delay Theory of Fully Capacitive Δ-Network

Fayu Wan, Yang Liu, Jamel Nebhen, Zhifei Xu, George Chan, Sebastien Lallechere, Remy Vauche, Wenceslas Rahajandraibe, Blaise Ravelo

IEEE Access
Multidisciplinary | Rapid Review | Open Access Journal

Received March 26, 2021, accepted April 8, 2021, date of publication April 12, 2021, date of current version April 29, 2021.

Digital Object Identifier 10.1109/ACCESS.2021.3072485

Bandpass Negative Group Delay Theory of Fully Capacitive Δ-Network

FAYU WAN[1], (Member, IEEE), YANG LIU[2], JAMEL NEBHEN[3], (Member, IEEE), ZHIFEI XU[4], (Member, IEEE), GEORGE CHAN[5], (Senior Member, IEEE), SÉBASTIEN LALLÉCHÈRE[6], (Member, IEEE), RÉMY VAUCHE[7], (Member, IEEE), WENCESLAS RAHAJANDRAIBE[7], (Member, IEEE), AND BLAISE RAVELO[1], (Member, IEEE)

[1]School of Electronic and Information Engineering, Nanjing University of Information Science and Technology, Nanjing 210044, China
[2]Altran, 78140 Vélizy-Villacoublay, France
[3]College of Computer Engineering and Sciences, Prince Sattam Bin Abdulaziz University, Alkharj 11942, Saudi Arabia
[4]EMC Laboratory, Missouri University of Science and Technology, Rolla, MO 65401, USA
[5]ASM Pacific Technology Ltd., Hong Kong
[6]Universitè Clermont Auvergne, CNRS, SIGMA Clermont, Institut Pascal, F-63000 Clermont-Ferrand, France
[7]IM2NP, CNRS, Université de Toulon, Aix-Marseille University, 13397 Marseille, France

Corresponding author: Zhifei Xu (zxfdc@mst.edu)

This work was supported in part by the NSFC under Grant 61971230, in part by the Jiangsu Specially Appointed Professor Program and Six Major Talents Summit of Jiangsu Province under Grant 2019-DZXX-022, in part by the Startup Foundation for Introducing Talent of NUIST, and in part by the Postgraduate Research and Practice Innovation Program of Jiangsu Province under Grant KYCX20_0966.

ABSTRACT A particularly original negative group delay (NGD) theory of Δ-topology is developed in the present paper. The NGD three-port topology is a passive circuit purely constituted by capacitors network. The model of the proposed Δ-topology impedance 3-D matrix is analytically established in function of the capacitor elements. Then, the S-matrix model is derived by using the Y-to-S transform. By considering the S-matrix frequency responses, a bandpass (BP) NGD analysis of the capacitive Δ-topology is originally elaborated. It is theoretically demonstrated that the passive Δ-topology is susceptible to behave as a BP NGD circuit under an analytical condition between the constituting capacitor values. The design feasibility of the BP NGD function is experimentally verified with lumped capacitor components-based Δ-circuit proof of concept. An electronic circuit board constituted by purely capacitive-network Δ-circuit is fabricated as an original Δ-circuit prototype. The tested board is constituted by arbitrary chosen capacitors, 100 nF, 10 nF and 0.1 nF. As expected, the calculation, simulation and measurement results, which are in very good agreement, confirm the BP NGD behavior. It is observed from measurement that it generates NGD of about −18.1 ns at a frequency of about 0.55 MHz and, lower and upper cut-off frequencies of about 0.33 MHz and 1.71 MHz. It is noteworthy that the transmission and reflection coefficients at very low frequency are independent of the capacitor values and analytically equal to 2/3 and 1/3, respectively.

INDEX TERMS Bandpass (BP) negative group delay (NGD), passive topology, Δ-topology, three-port circuit, S-parameter modeling, NGD theory, capacitive network.

I. INTRODUCTION

The first experimentations of the negative group delay (NGD) effect were realized in 1980s with optical system [1], [2]. These experimentations were initially based on the consideration of negative group velocity (NGV) dispersive media [1]–[4]. The NGD experimental extraordinary demonstrations were occasionally made with short duration pulses propagating in the optical systems [5]–[7]. The NGD effect was classified among anomalous physical phenomenon [8]. It was found that the time-domain signature of the NGD effect manifests with the propagation of the output pulse in time-advance compared to its input [1]–[9]. Thanks to the time-advance behavior, the NGD investigation enables also to verify some extraordinary physical effects as superluminal pulse propagation [9]. Therefore, the interpretation of the NGD effect intrigues optical and electronic physicists. Despite the counterintuitive NGD effect, it was underlined

The associate editor coordinating the review of this manuscript and approving it for publication was Pavlos I. Lazaridis.

theoretically and experimentally that the causality is always respected [10]–[12].

The understanding curious questions about the NGV behaviors attracted also the attention of radio frequency (RF) and microwave design engineers in early 2000s. Some revolutionary designs were made with NGV structures based on the negative refractive index metamaterial and left-handed structures [13]–[20]. The metamaterial NGD circuits were usually implemented with split ring resonator (SRR) structures [13], [18]. Moreover, several periodical SRR cells [14], [16] are necessary to generate significant NGD values with some minus nanoseconds.

Some tentative applications of NGD microwave circuits for the enhancement of amplifier linearity [21], independent frequency phase shifter [22], antenna array [23]–[24], printed circuit board (PCB) interconnect effect on signal delay [25], GD equalization [26] and non-Foster negative capacitor [27] were proposed. Nevertheless, the NGD circuit design present certain challenges in terms of the understandability, complexity and attenuation loss for many of RF and microwave design engineers. Therefore, the design interests of microwave engineers decrease because of significant attenuation loss (which can be more than 30 dB) and the design complexity of NRI metamaterial based NGD circuits.

To overcome this technical limitation, some few groups of worldwide [28]–[47] of RF and microwave design researchers wondered about the design feasibility of low attenuation and simpler topologies of NGD circuits. Distributed NGD topology was proposed with second-order RC circuit configurations [28]. NGD passive topology with resonator approach was also investigated [29]. More complex NGD circuit based on the interference technique was also designed [30]. A new generation of NGD microstrip passive circuits [31]–[37] inspired from metamaterial designs were made in 2010s. One of the most developed low-attenuation NGD topologies is based on the use of microstrip coupled transmission lines (TLs) [31]–[34]. Some outstandingly compact microstrip circuits operating with NGD function [35]–[37] were also introduced. Against the loss limitation, some active topologies of NGD low frequency (LF) and microwave circuits were also introduced [38]–[43]. Despite the different exploratory studies on the electronic circuit designs, the NGD function is still not familiar to majority of electronic design engineers. Therefore, a simple and easier to understand manner to theorize the NGD function must be developed.

Accordingly, a simple to understand NGD function theory was established based on the similitude between the filter function [44]. The similitude is related to the analogy between the behavior of the magnitude and GD of causal linear circuits. In difference with the filters, the NGD functions are characterized based on the frequency bands where the sign of the GD is negative. Some elementary topologies of low-pass (LP) [45], high-pass (HP) [46] and bandpass (BP) [47] NGD circuits were initiated. Following this innovative NGD theorization, we can understand that the previously described metamaterial inspired, coupled line and compact NGD microwave circuits [19]–[37] are classified as BP NGD function. However, in difference to the other electronic functions (filter, attenuators, phase shifters, amplifiers, power combiner, power dividers, ...) if we summarize and classify all the NGD topologies existing in the literature [1]–[47], they are limited to the following characteristics:

- Two port topologies,
- Resistive, inductive and capacitive (LC) network circuit topologies,
- And resonance microstrip TL based topologies.

By curiosity, we are wondering about the designability of NGD passive lumped topology constituted by three-port and mono-nature circuits. The main originality of the present research work is the modelling, design and test of passive Δ-topology composed by only capacitive networks. The present paper is dealing to the answer of this curious question by developing an original three-port circuit constituted by Δ-topology composed only by capacitive network without resistor and inductor elements. The proposed paper is organized in four different sections:

- Section II is focused on the S-parameter modelling of the tri-port passive Δ-topology. The considered model is analytically elaborated by the exploration of the Kirchhoff voltage and current laws.
- Section III presents the BP NGD analysis from the transmission coefficient identification. The main specifications of the BP NGD function from the Δ-topology are expressed.
- Section IV describes the validation results by comparison of the analytical model, simulation and experimental measurement. A proof of concept (POC) design will be introduced and the test results of the fabricated prototype will be discussed.
- Section V ends the paper with conclusion.

II. S-MATRIX MODELLING OF THE Δ-TOPOLOGY

The present section introduces the analytical theory on the S-matrix modelling. The established theory is based on the three-port circuit represented by Δ-topology. The modelling is established based on the Kirchhoff voltage and current laws.

A. TOPOLOGICAL DESCRIPTION

To elaborate the analytical model of the purely capacitive Δ-topology under study, we propose to start with the preliminary diagram description in the following paragraph.

1) GENERAL REPRESENTATION

The tri-port topology under study is represented by the Δ-circuit depicted in Fig. 1. The circuit is fed by three voltage sources, $U_{k=1,2,3}$, which are connected at port, k via node M_k with $k = 1, 2, 3$. We recall that the main originality of the present study is based on the consideration of Δ-shape tri-port topology. Each branch of the topology is constituted by series impedance which are composed of purely capacitive network.

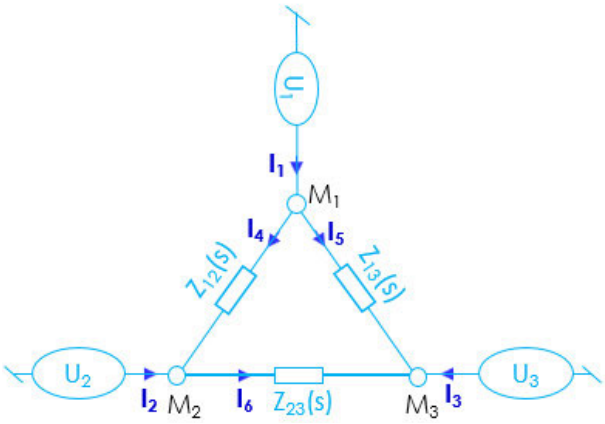

FIGURE 1. Δ-topology of the tri-port circuit under study.

The two-port impedance elements constituting the Δ-circuit under study are represented by the capacitors connected in three branches M_1M_2, M_1M_3 and nodes M_2M_3 denoted by:

$$\begin{cases} Z_{12}(s) = \dfrac{1}{C_{12}s} \\ Z_{13}(s) = \dfrac{1}{C_{13}s} \\ Z_{23}(s) = \dfrac{1}{C_{23}s} \end{cases} \tag{1}$$

with the different series capacitors $C_{k=12,13,23}$ and Laplace variable, s. By proceeding similar to the impedance matrix extraction introduced in [37], the admittance matrix of Δ-topology is defined by the generalized Ohm's relationship:

$$[I(s)] = [Y(s)] \times [U(s)] \tag{2}$$

where the vector current and vector voltage:

$$[I(s)] = \begin{bmatrix} I_1(s) \\ I_2(s) \\ I_3(s) \end{bmatrix} \tag{3}$$

$$[U(s)] = \begin{bmatrix} U_1(s) \\ U_2(s) \\ U_3(s) \end{bmatrix}. \tag{4}$$

Before the analytical investigation, let us describe the block system representation in the next paragraph.

2) BLOCK SYSTEM REPRESENTATION

To make easier the didactical analysis, the capacitive Δ-topology can be represented as a three-port system. Therefore, we can assume the equivalent diagram depicted by Fig. 2.

The main objective of this analytical investigation is to determine the expression of the equivalent 3-D S-matrix model [S] in function of the constituting branch impedances. Based on the S-parameter and circuit theory, the equivalent model of the Δ-topology can be expressed by the following

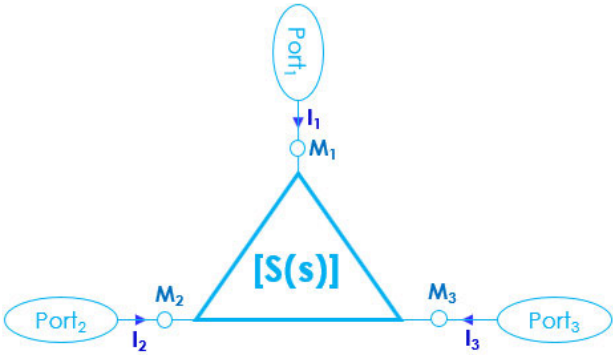

FIGURE 2. Tri-port system representation of the Δ-topology introduced in Fig. 1.

S-matrix:

$$[S(s)] = \begin{bmatrix} S_{11}(s) & S_{12}(s) & S_{13}(s) \\ S_{21}(s) & S_{22}(s) & S_{23}(s) \\ S_{31}(s) & S_{32}(s) & S_{33}(s) \end{bmatrix}. \tag{5}$$

Acting as a tri-port passive circuit, we have the simplification:

$$\begin{cases} S_{12}(s) = S_{21}(s) \\ S_{13}(s) = S_{31}(s) \\ S_{23}(s) = S_{32}(s) \end{cases}. \tag{6}$$

Based on the KCLs, the coefficients of the matrix will be determined in the following subsection.

B. ANALYTICAL S-PARAMETER MODELLING OF Δ-TOPOLOGY

The mathematical demonstration of the capacitive Δ-topology admittance matrix model is developed in the following paragraph. Based on the Y-to-S matrix transform, the S-parameter equivalent model will be derived.

1) ADMITTANCE MATRIX CALCULATION

By application of the node KCL at M_1, M_2 and M_3, we have the following system equations, respectively:

$$\begin{cases} I_1(s) = I_4(s) + I_5(s) \\ I_2(s) = I_6(s) - I_4(s) \\ I_3(s) = -I_5(s) - I_6(s) \end{cases}. \tag{7}$$

The Ohm's laws applied to branches M_1M_2, M_1M_3 and M_2M_3, of the Δ-circuit enables to write the system equations, respectively:

$$\begin{cases} U_1(s) - U_2(s) = Z_{12}(s)I_4(s) \\ U_1(s) - U_3(s) = Z_{13}(s)I_5(s) \\ U_2(s) - U_3(s) = Z_{23}(s)I_6(s) \end{cases}. \tag{8}$$

Substituting, the expressions of current, I_4 and I_5 from equation (8) into the first equation of system (7), it can be derived in function of the voltage sources:

$$I_1(s) = \left[\frac{1}{Z_{12}(s)} + \frac{1}{Z_{13}(s)}\right] U_1(s) - \frac{U_2(s)}{Z_{12}(s)} - \frac{U_3(s)}{Z_{13}(s)}. \tag{9}$$

The same substitution applied to the second and third equations of system (8) implies the following expressions of currents, I_2 and I_3, respectively:

$$I_2(s) = \left[\frac{1}{Z_{12}(s)} + \frac{1}{Z_{23}(s)}\right] U_2(s) - \frac{U_1(s)}{Z_{12}(s)} - \frac{U_3(s)}{Z_{23}(s)} \quad (10)$$

$$I_3(s) = -\frac{U_1(s)}{Z_{13}(s)} - \frac{U_2(s)}{Z_{23}(s)} + \left[\frac{1}{Z_{13}(s)} + \frac{1}{Z_{23}(s)}\right] U_3(s). \quad (11)$$

By identification with the matrix relationship given by equation (2), the admittance matrix of the Δ-topology can be expressed by:

$$[Y(s)] = \begin{bmatrix} Y_{11}(s) & \frac{-1}{Z_{12}(s)} & \frac{-1}{Z_{13}(s)} \\ \frac{-1}{Z_{12}(s)} & Y_{22}(s) & \frac{-1}{Z_{23}(s)} \\ \frac{-1}{Z_{13}(s)} & \frac{-1}{Z_{23}(s)} & Y_{33}(s) \end{bmatrix} \quad (12)$$

with:

$$Y_{11}(s) = \frac{1}{Z_{12}(s)} + \frac{1}{Z_{13}(s)} \quad (13)$$

$$Y_{22}(s) = \frac{1}{Z_{12}(s)} + \frac{1}{Z_{23}(s)} \quad (14)$$

$$Y_{33}(s) = \frac{1}{Z_{13}(s)} + \frac{1}{Z_{23}(s)}. \quad (15)$$

2) S-MATRIX CALCULATION

Thanks to the Y-to-S matrix transform, the S-matrix extraction was performed via the relationship:

$$[S(s)] = \left\{\left[Y_{ref}\right] - [Y(s)]\right\} \times \left\{\left[Y_{ref}\right] + [Y(s)]\right\}^{-1} \quad (16)$$

by denoting $R_0 = 50\Omega$, the general reference impedance of access ports can be written as:

$$\left[Y_{ref}\right] = \begin{bmatrix} 1/R_0 & 0 & 0 \\ 0 & 1/R_0 & 0 \\ 0 & 0 & 1/R_0 \end{bmatrix}. \quad (17)$$

Accordingly, we have the reflection coefficients expressed as:

$$S_{11}(s) = \frac{Z_{12}(s)Z_{13}(s)\left[2R_0 + Z_{23}(s)\right] - R_0^2\left[Z_{12}(s) + Z_{13}(s) + Z_{23}(s)\right]}{D(s)} \quad (18)$$

$$S_{22}(s) = \frac{Z_{12}(s)Z_{23}(s)\left[2R_0 + Z_{13}(s)\right] - R_0^2\left[Z_{12}(s) + Z_{13}(s) + Z_{23}(s)\right]}{D(s)} \quad (19)$$

$$S_{33}(s) = \frac{Z_{13}(s)Z_{23}(s)\left[2R_0 + Z_{12}(s)\right] - R_0^2\left[Z_{12}(s) + Z_{13}(s) + Z_{23}(s)\right]}{D(s)} \quad (20)$$

with the denominator:

$$D(s) = \left\{\begin{array}{c} 3R_0^2\left[Z_{12}(s) + Z_{13}(s) + Z_{23}(s)\right] \\ +2R_0Z_{12}(s)\left[Z_{13}(s) + Z_{23}(s)\right] \\ +Z_{13}(s)Z_{23}(s)\left[R_0 + Z_{12}(s)\right] \end{array}\right\}. \quad (21)$$

Then, the Δ-topology transmission coefficients are given by:

$$S_{21}(s) = \frac{2R_0\left\{\begin{array}{l} R_0\left[Z_{12}(s) + Z_{13}(s) + Z_{23}(s)\right] \\ +Z_{13}(s)Z_{23}(s) \end{array}\right\}}{D(s)} \quad (22)$$

$$S_{31}(s) = \frac{2R_0\left\{\begin{array}{l} R_0\left[Z_{12}(s) + Z_{13}(s) + Z_{23}(s)\right] \\ +Z_{12}(s)Z_{23}(s) \end{array}\right\}}{D(s)} \quad (23)$$

$$S_{32}(s) = \frac{2R_0\left\{\begin{array}{l} R_0\left[Z_{12}(s) + Z_{13}(s) + Z_{23}(s)\right] \\ +Z_{12}(s)Z_{13}(s) \end{array}\right\}}{D(s)}. \quad (24)$$

Based on these S-matrix expressions, BP NGD analysis will be performed in the next section.

III. BP NGD ANALYSIS AND SPECIFICATIONS

Because of its counterintuitive effect, the BP NGD function still remains unfamiliar to most of electronic design engineers. Therefore, it would be necessary to define in the most understandable way the methodology of the BP NGD analysis.

A. FREQUENCY RESPONSES REQUIRED FOR THE NGD STUDY

Similar to the classical electronic circuit analysis, the frequency responses of the Δ-topology are based on the consideration of the angular frequency variable, $s = j\omega$. The main transmittances are therefore expressed as $S_{km}(j\omega)$ with $k, m = 1, 2, 3$.

1) MAGNITUDE

During the NGD analysis, it is important to express analytically the magnitudes of the S-parameter coefficients. Knowing the reflection and transmission coefficients given in equations (18)-(20) and equation (22)-(24), the magnitudes are generally defined by:

$$S_{km}(\omega) = |S_{km}(j\omega)| = \frac{\sqrt{Rn_{km}^2(\omega) + In_{km}^2(\omega)}}{\sqrt{Rd_{km}^2(\omega) + Id_{km}^2(\omega)}} \quad (25)$$

where the quantities constituting the numerator and denominator:

$$\begin{cases} Rn_{km}(\omega) = Re\left\{numerator\left[S_{km}(j\omega)\right]\right\} \\ In_{km}(\omega) = Im\left\{numerator\left[S_{km}(j\omega)\right]\right\} \\ Rd_{km}(\omega) = Re\left\{denom\left[S_{km}(j\omega)\right]\right\} \\ Id_{km}(\omega) = Im\left\{denom\left[S_{km}(j\omega)\right]\right\} \end{cases} \quad (26)$$

with real (Re) and imaginary (Im) parts.

2) GD DEFINITION

The GD expressions of the Δ-topology are extracted from the transmission phases, for $k \neq m$, all are identical:

$$\varphi_{km}(\omega) = \arg\left[S_{km}(j\omega)\right]. \quad (27)$$

By taking the quantities defined by equation (26), the transmission phases can be rewritten as:

$$\varphi_{km}(\omega) = \arctan\left[\frac{In_{km}(\omega)}{Rn_{km}(\omega)}\right] - \arctan\left[\frac{Id_{km}(\omega)}{Rd_{km}(\omega)}\right]. \quad (28)$$

The associated GD is defined by:

$$GD_{km}(\omega) = \frac{-\partial\varphi_{km}(\omega)}{\partial\omega}. \quad (29)$$

Knowing these frequency response parameter definitions, we can propose the BP NGD function specifications in the following paragraphs.

B. BP NGD FUNCTION SPECIFICATIONS

The analysis of BP NGD function of the Δ-topology requires the understanding of the basic parameters as described in the following steps.

1) STEP1: NGD EXISTENCE CONDITION

The initial step of the BP NGD analysis consists in verifying the NGD existence condition. The mathematical inequation can be analytically formulated by with unknown the interval of ω:

$$GD(\omega) < 0. \quad (30)$$

In the case where this condition is not satisfied, the system belongs to the positive group delay (PGD) class. That means the system cannot behave as an NGD function and this is the final conclusion of the analysis.

2) STEP2: NGD VALUE

The NGD value can be defined from NGD center angular frequency, ω_o. There are several manners to define analytically this particular frequency. For example, at which frequency, the GD can reach its minimal negative value:

$$GD_{\min} = GD(\omega_o) < 0. \quad (31)$$

For the case of $\omega_o \neq 0$, the circuit belongs to the class of BP NGD behavior. Nevertheless, for many cases of NGD circuits [19]–[37], [47], it may be difficult to determine the exact expression of ω_o satisfying equation (31). Or we can also choose this center frequency as particular value defined with different analytical equation.

3) STEP3: NGD BANDWIDTH

Fig. 3 represents a representation of GD ideal response from the BP NGD function. In the present paper, the NGD center frequency is denoted ω_o whereas the NGD cut-off frequencies are ω_a and ω_b, which are the roots of equation:

$$GD(\omega) = 0. \quad (32)$$

As seen in Fig. 3, we take, for example, $\omega_a < \omega_b$. The NGD bandwidth can be determined by the relation:

$$\Delta\omega_{NGD} = \omega_b - \omega_a. \quad (33)$$

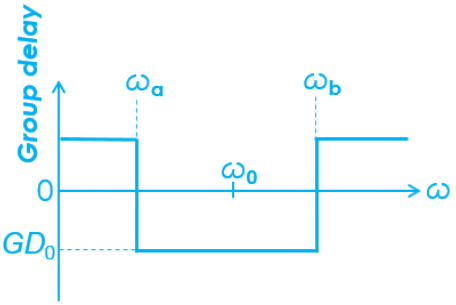

FIGURE 3. Ideal response of BP NGD function.

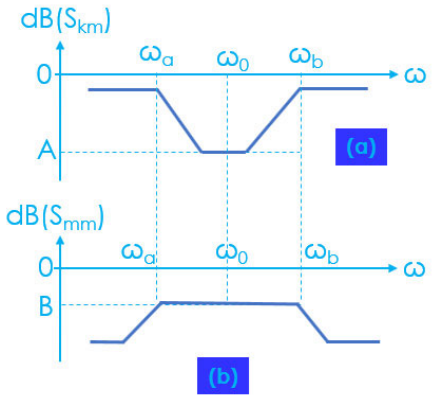

FIGURE 4. Ideal response of (a) transmission and (b) reflection coefficients.

The GD response of BP NGD function is ideally specified by:

$$\begin{cases} GD(\omega < \omega_a) > 0 \\ GD(\omega_a < \omega < \omega_b) < 0 \\ GD(\omega_b < \omega) > 0 \end{cases}. \quad (34)$$

In addition to the GD response, the BP NGD analysis depends also on the reflection and transmission coefficient specifications.

4) STEP4: REFLECTION AND TRANSMISSION COEFFICIENTS

Figs. 4 introduces the ideal representation of the transmission and reflection coefficients of typical BP NGD circuit. Within the NGD bandwidth, the attenuation related to the transmission coefficient and the access matching of the Δ-topology must respect certain limitations. For example, we can denote the attenuation limit, A, according to the targeted field of applications.

Subsequently, the NGD loss can be formulated with the following condition:

$$S_{km}(\omega) \geq [S_{km}(\omega)]_{\min} = A. \quad (35)$$

In addition, the inverse condition must be checked if the targeted application system is sensitive to access mismatching. The reflection coefficient must satisfy the following condition for a given maximal reflection limit denoted B. This matching level is mostly fixed at −10 dB according to RF and microwave engineering standards. The reflection coefficient

condition can be formulated as:

$$S_{mm}(\omega) \leq [S_{mm}(\omega)]_{\max} = B. \tag{36}$$

During the analytical calculation, both conditions versus the NGD center frequency are usually merged as:

$$\begin{cases} S_{km}(\omega_o) = A \\ S_{mm}(\omega_o) = B \end{cases}. \tag{37}$$

The practical BP NGD analysis of the Δ-topology from the previous expressions of the S-parameters will be established in the following section.

IV. BP NGD THEORETICAL CHARACTERIZATION OF THE CAPACITIVE NETWORK BASED Δ-TOPOLOGY

The theoretical detailed approach on the BP NGD analysis of the Δ-topology is explored in the present section. First, the BP NGD specifications are defined. Then, the transmission coefficients are identified by the BP NGD canonical form [47].

A. S-PARAMETER COEFFICIENTS IN FUNCTION OF THE CAPACTIVE ELEMENTS

The detailed expressions of the S-parameters in function of the capacitive elements are expressed by considering the impedance of equation (1). Accordingly, the reflection coefficients introduced by equations (18), (19) and (20) become respectively:

$$S_{11}(s) = \frac{1 + 2R_0C_{23}s - R_0^2\left[C_{12}(C_{13} + C_{23}) + C_{13}C_{23}\right]s^2}{D(s)} \tag{38}$$

$$S_{22}(s) = \frac{1 + 2R_0C_{13}s - R_0^2\left[C_{12}(C_{13} + C_{23}) + C_{13}C_{23}\right]s^2}{D(s)} \tag{39}$$

$$S_{33}(s) = \frac{1 + 2R_0C_{12}s - R_0^2\left[C_{12}(C_{13} + C_{23}) + C_{13}C_{23}\right]s^2}{D(s)} \tag{40}$$

with:

$$D(s) = \begin{Bmatrix} 3R_0^2\left[C_{12}(C_{13} + C_{23}) + C_{13}C_{23}\right]s^2 \\ +2R_0(C_{12} + C_{13} + C_{23})s + 1 \end{Bmatrix}. \tag{41}$$

Similarly, the analytical expressions of the transmission coefficients can be written as:

$$S_{21}(s) = \frac{2R_0s\left[C_{12}(1 + R_0C_{13}s) + R_0C_{23}s(C_{12} + C_{13})\right]}{D(s)} \tag{42}$$

$$S_{31}(s) = \frac{2R_0s\left[C_{13}(1 + R_0C_{12}s) + R_0C_{23}s(C_{12} + C_{13})\right]}{D(s)} \tag{43}$$

$$S_{32}(s) = \frac{2R_0s\left[C_{23}(1 + R_0C_{12}s) + R_0C_{23}s(C_{12} + C_{13})\right]}{D(s)}. \tag{44}$$

The analytical identification of the BP NGD class will be elaborated in the following subsection.

B. BP NGD INVESTIGATION VIA CANONICAL FORM IDENTIFICATION

The BP NGD analysis of the capacitive Δ-topology can be performed by considering the transmission coefficient canonical form. The following paragraph presents the identification of the parameters.

1) CANONICAL FORM

To identify the adequate transmission coefficient expression, an adequate TF canonical form needs to be developed. For example, the canonical form associated to the elementary BP NGD TFs associated to transmission coefficients introduced in equations (42) and (43) can be defined by the second order polynomial formula:

$$T(s) = \frac{T_0s(s + n_1)}{s^2 + d_1s + d_0}. \tag{45}$$

By identification with transmission coefficients, S_{21}, S_{31}, and S_{32}, expressed in equations (42), (43), and (44), we have $T_0 = 2/3$ and the numerator parameters, respectively:

$$\begin{cases} n_1(S_{21}) = \dfrac{C_{12}}{R_0\left[C_{12}(C_{13} + C_{23}) + C_{13}C_{23}\right]} \\ n_1(S_{31}) = \dfrac{C_{13}}{R_0\left[C_{12}(C_{13} + C_{23}) + C_{13}C_{23}\right]} \\ n_1(S_{32}) = \dfrac{C_{23}}{R_0\left[C_{12}(C_{13} + C_{23}) + C_{13}C_{23}\right]} \end{cases} \tag{46}$$

and the common denominator parameters:

$$d_1 = \frac{2(C_{12} + C_{13} + C_{23})}{3R_0\left[C_{12}(C_{13} + C_{23}) + C_{13}C_{23}\right]} \tag{47}$$

$$d_0 = \frac{1}{3R_0^2\left[C_{12}(C_{13} + C_{23}) + C_{13}C_{23}\right]}. \tag{48}$$

The TF canonical form presents the frequency responses analytically expressed in the following paragraph.

2) FREQUENCY RESPONSES

The main quantities of the frequency responses to be studied in this subsection are given in subsection III-A without considering the reflection coefficient. The magnitude corresponding to the canonical form given by equation (45) can be written as:

$$T(\omega) = \frac{T_0\omega\sqrt{n_1^2 + \omega^2}}{\sqrt{(d_0 - \omega^2)^2 + d_1^2\omega^2}}. \tag{49}$$

The associated to TF transmission phase derived from equation (20) is given by:

$$\varphi(\omega) = \arctan\left(\frac{\omega}{n_1}\right) - \arctan\left(\frac{d_1\omega}{d_0 - \omega^2}\right). \tag{50}$$

The GD defined in equation (21) becomes:

$$GD(\omega) = \frac{\zeta_4\omega^4 + \zeta_2\omega^2 + \zeta_0}{(\omega^2 + n_1^2)\left[\omega^4 + (d_1^2 - 2d_0)\omega^2 + d_0^2\right]} \tag{51}$$

with:

$$\begin{cases} \zeta_0 = n_1 d_0 (n_1 d_1 - d_0) \\ \zeta_2 = d_0 (n_1 + d_1) + n_1 d_1 (n_1 - d_1) \\ \zeta_4 = d_1 - n_1 \end{cases} . \quad (52)$$

By analytically examining this GD, the NGD aspect of the capacitive Δ-topology is analytically characterized in the following paragraph.

3) BP NGD CHARACTERIZATION

By solving equation (32) with the previously established GD, we obtain the following cut-off frequencies:

$$\omega_a = \frac{\sqrt{d_0(d_1 + 2n_1) + n_1 d_1 (n_1 - d_1) - d_1 \left[n_1 (n_1 - d_1) + d_0 \right] \sqrt{\Delta_\omega}}}{\sqrt{2(d_1 - n_1)}} \quad (53)$$

$$\omega_b = \frac{\sqrt{d_0(d_1 + 2n_1) + n_1 d_1 (n_1 - d_1) + d_1 \left[n_1 (n_1 - d_1) + d_0 \right] \sqrt{\Delta_\omega}}}{\sqrt{2(d_1 - n_1)}} \quad (54)$$

with:

$$\Delta_\omega = d_0(8n_1 + d_1) + n_1 d_1 (n_1 - d_1). \quad (55)$$

The analytical expression of the product of these cut-off frequencies is equal to:

$$\omega_a \omega_b = \frac{\sqrt{d_0 n_1 (n_1 d_1 - d_0)}}{\sqrt{d_1 - n_1}}. \quad (56)$$

We naturally proceed under condition:

$$\omega_a < \omega_o < \omega_b \quad (57)$$

to choose the NGD center frequency:

$$\omega_0 = \sqrt{d_0}. \quad (58)$$

By considering equation (48), we have:

$$\omega_0 = \frac{1}{R_0 \sqrt{3(C_{12}(C_{13} + C_{23}) + C_{13} C_{23})}}. \quad (59)$$

It yields the GD expressed previously in equation (51) simplified as:

$$GD(\omega_0) = \frac{2n_1^2 - n_1 d_1 + 2d_0}{d_1 (n_1^2 + d_0)}. \quad (60)$$

This last relation explains that if:

$$d_0 < n_1 \left(\frac{d_1}{2} - n_1 \right) \quad (61)$$

The capacitive Δ-topology behaves as a BP NGD function. Moreover, the transmission coefficient magnitude given in equation (49) will be reduced to:

$$T(\omega_0) = \frac{2\sqrt{d_0 (n_1^2 + d_0^2)}}{3 d_1 \sqrt{d_0}}. \quad (62)$$

The design and NGD behavioral feasibility by designing of POC with purely capacitive network Δ-circuit will be investigated in the next section.

V. DISCUSSION ON CALCULATED, SIMULATED AND EXPERIMENTED RESULTS OF Δ-TOPOLOGY

The relevance of the innovative BP NGD theory associated to our tri-port Δ-topology established in the previous section is verified in the present one.

A POC of Δ-circuit prototype was designed, modelled, simulated, fabricated and tested to validate the BP NGD behavior. The modelling analytical equations are calculated from the MATLAB® computations by exploiting:

- the reflection coefficients previously established in equation (38), equation (39) and equation (40),
- the transmission coefficients previously established in equation (42), equation (43) and equation (44),
- and the GDs generalized by equation (51).

Then, the calculated results will be compared with simulations and measurements. The simulations were generated by the circuit design in the schematic environment of the electronic circuit designer and simulator ADS® from Keysight Technologies®.

Before the exploration of the validation results, the Δ-circuit POC design will be described in the following paragraph.

A. DESCRIPTION OF THE Δ-CIRCUIT POC PROTOTYPES

The ADS® design schematic of the capacitive Δ-circuit prototype of tri-port topology constituted only by passive network is displayed in Fig. 5(a). The Δ-circuit schematic indicates the simulated component values, excitation ports, $port_1$, $port_2$ and $port_3$, and also the simulated frequency parameters. $R_0 = 50\Omega$ represents the reference impedance of each excitation port. This POC was parametrized with capacitor components available in our laboratory and also allowing to demonstrate the feasibility of the BP NGD behavior. The photograph of the tested electronic circuit board is displayed by Fig. 5(b). It can be emphasized that the Δ-circuit prototype was designed and fabricated with only capacitor components. The PCB POC is implemented on Cu-metalized FR4 dielectric substrate in hybrid technology. It is noteworthy that in difference to the existing NGD circuits [13-44,45], we emphasize that this Δ-circuit prototype is originally designed as a three-port PCB which is only constituted by capacitors with no resistive and inductive elements.

The parameters of POC constituting the fabricated Δ-circuit prototype are indicated in Table 1.

The following subsection explores the comparative validation results from the S-parameter magnitudes and also the GDs.

B. DISCUSSION ON THE BP NGD RESPONSE VALIDATION RESULTS

The present subsection introduces the comparison between the calculated model, simulated and experimented results of the fabricated Δ-circuit prototype. The validation is essentially examined by comparison of S-parameters. The validation analysis explored in the following paragraphs

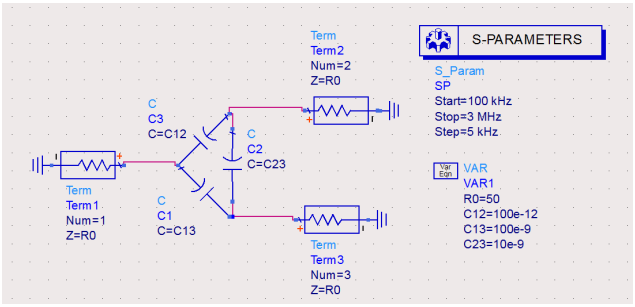

(a)

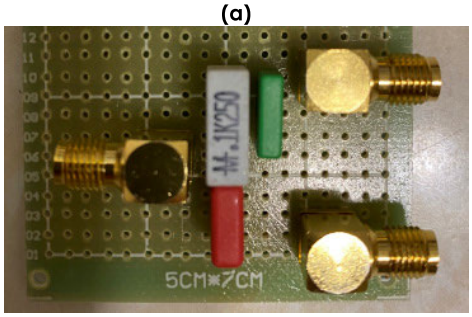

(b)

FIGURE 5. (a) Schematic and (b) photograph of the POC of Δ-circuit prototype.

TABLE 1. Parameters of the components constituting the Δ-circuit prototype.

Type	Construction technology	Nominal value	Tolerance
Capacitor	Polypropylene	C_{12}=100 pF	+/- 5%
		C_{13}=100 nF	
		C_{23}=10 nF	

is carried out in the frequency band defined from 200 kHz to 3 MHz.

1) EXPERIMENTAL SETUP DESCRIPTION

The test of the capacitive Δ-topology POC prototype was carried out similar to the classical RF and microwave circuits. The illustrative diagram of the test is proposed in Figs. 6.

The measurement of the S-parameters was carried out in three-port configuration.

The measurement was done with a Vector Network Analyzer (VNA) as illustrated by the experimental setup shown in the photograph of Figs. 6. The employed four-port VNA is referenced ENA Series E5071C from Keysight Technologies® which has frequency band delimited from 9 kHz to 8.5 GHz. The S-parameter measurement test was made under SOLT calibration.

The next paragraphs examine the measured reflection and transmission coefficients and also the GDs compared with the calculation and simulation.

2) REFLECTION S-PARAMETER RESULTS

The first step of NGD behavior of the Δ-circuit POC, comparisons between calculated (“Calc.”), simulated (“Simu.”), and measured (“Meas.”) reflection coefficients

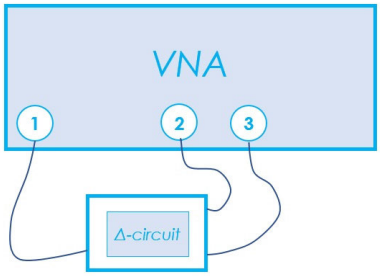

(a)

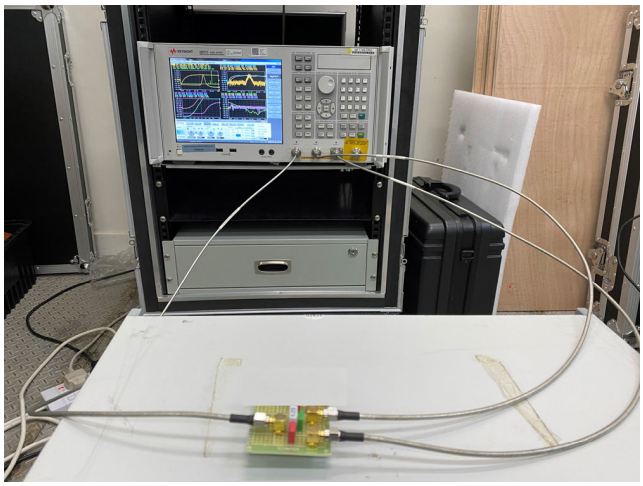

(b)

FIGURE 6. Configuration of the passive Δ-circuit prototype experimental setup.

are introduced in this paragraph. Accordingly, the calculated, simulated and measured results are displayed by Figs. 7 in red dotted cyan, solid black and dashed red curves, respectively.

The obtained reflection coefficients, S_{11}, S_{22} and S_{33} are depicted by Fig. 7(a), Fig. 7(b) and Fig. 7(c), respectively. It can be underlined that the calculated, simulated and measured results are in very good correlation in the considered operation frequency band.

The slight differences, notably for S_{22} seen from 1 MHz to 3 MHz, is essentially due to the tolerances and the parasitic effects of the employed R and C components. Based on these good agreements, we confirm the effectiveness of the established analytical model of reflection parameters proposed in equations (38), (39) and (40). The whole S-parameter validation will be performed in the next paragraph by considering the transmission coefficients.

3) TRANSMISSION S-PARAMETER RESULTS

As illustrated by equation (29), the GD responses are directly derived from the transmission coefficients, S_{KM} $(K, M = 1, 2, 3)$. Therefore, the validation of $S_{21} = S_{12}$, $S_{31} = S_{13}$ and $S_{32} = S_{23}$ are particularly relevant for the NGD investigation of Δ-circuit topology. Fig. 8(a), Fig. 8(b) and Fig. 8(c) represent the comparisons of calculated, simulated and measured transmission coefficients, S_{21}, S_{31}, and S_{32} of the Δ-circuit prototype, respectively. For the three cases

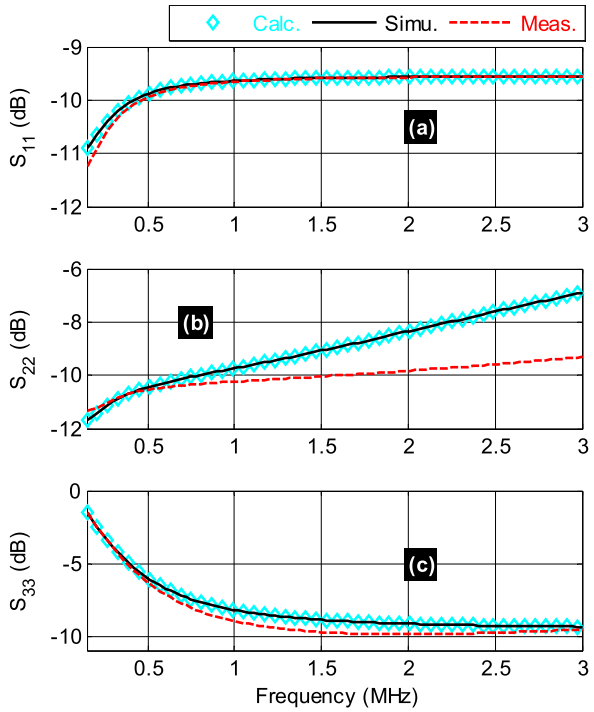

FIGURE 7. Comparisons between simulated, measured and calculated reflection coefficients of the Δ-circuit prototype: (a) S_{11}, (b) S_{22} and (c) S_{33}.

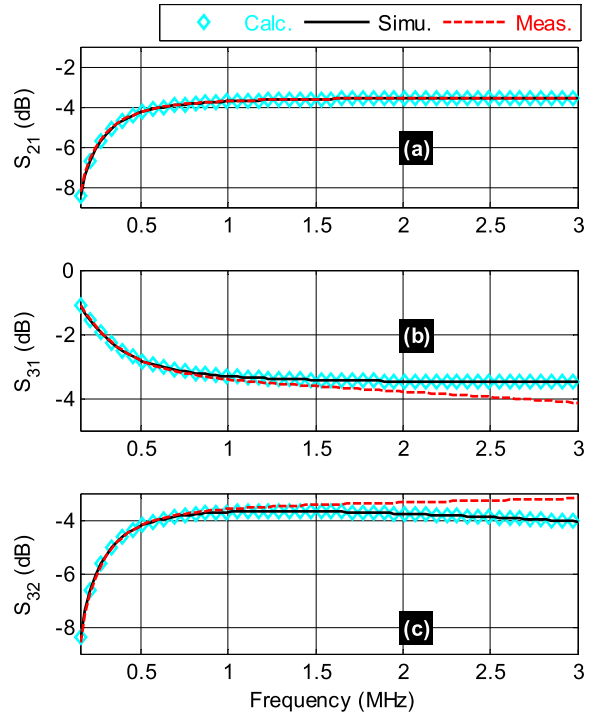

FIGURE 8. Comparisons between simulated, measured and calculated transmission coefficients of the Δ-circuit prototype: (a) S_{21}, (b) S_{31} and (c) S_{32}.

of the plot, the transmission parameters are well-correlated in the considered frequency range.

Thanks to the relevance between the simulated and experimented results, we can confirm the relevance of transmission

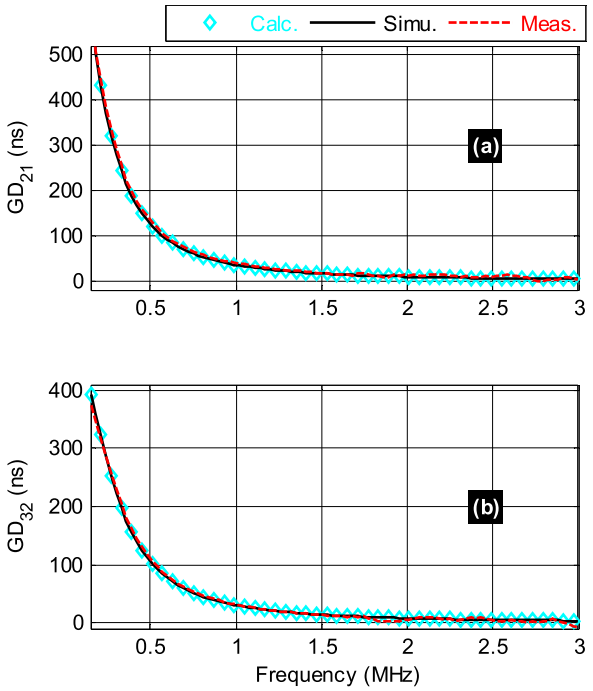

FIGURE 9. Comparisons between simulated, measured and calculated GDs from transmission coefficients, (a) S_{21} and (b) S_{32} of the Δ-circuit prototype.

coefficient models developed in equations (42), (43) and (44). To verify the BP NGD design feasibility of Δ-circuit, the comparative investigation of GD responses will be discussed in the following paragraph.

4) GD RESULTS

The present paragraph examines the GD comparative responses from the different transmission coefficients associated to our three-port Δ-circuit prototype.

Similar to the two previous paragraphs, the validation is based on the comparisons between the calculated ("Calc."), simulated ("Simu."), and measured ("Meas.") GDs expressed in equation (51). The plots of GD_{21} and GD_{32} are shown in Fig. 9(a) and Fig. 9(b), respectively. We can remark a very good correlation between the three different approaches in the whole frequency band. Nevertheless, the GD is always positive in for the transmission parameters between $port_1$ and $port_2$, and also $port_2$ and $port_3$ of t Δ-circuit prototype.

The BP NGD function innovative study of the present paper is confirmed by the result of GD_{31} plots depicted by Figs. 10. We can underline the calculated, simulated and measured GDs are in very good agreement. More importantly, we can see clearly in Fig. 10(b) that we have a BP NGD behavior. We can characterize the measured BP NGD response with NGD center frequency of approximately $f_0 = 0.55$ MHz and GD value of about $GD_0 = -18.1$ ns. Nevertheless, the measured GD presents an imperfection manifested by fluctuation noises compared to the simulated and calculated ones. This observed difference from the

TABLE 2. Comparison of BP NGD specifications from the GD associated to transmission coefficient S_{31}.

Validation approach	f_0	$GD_{31}(f_0)$	Δf	$S_{31}(f_0)$	$S_{11}(f_0)$
Calculated	0.51 MHz	-18.1 ns	5.75 MHz	-2.84 dB	-9.95 dB
Simulated	0.512 MHz	-18.05 ns	5.74 MHz	-2.842 dB	-9.95 dB
Measured	0.55 MHz	-18.12 ns	1.35 MHz	-2.95 dB	-9.83 dB

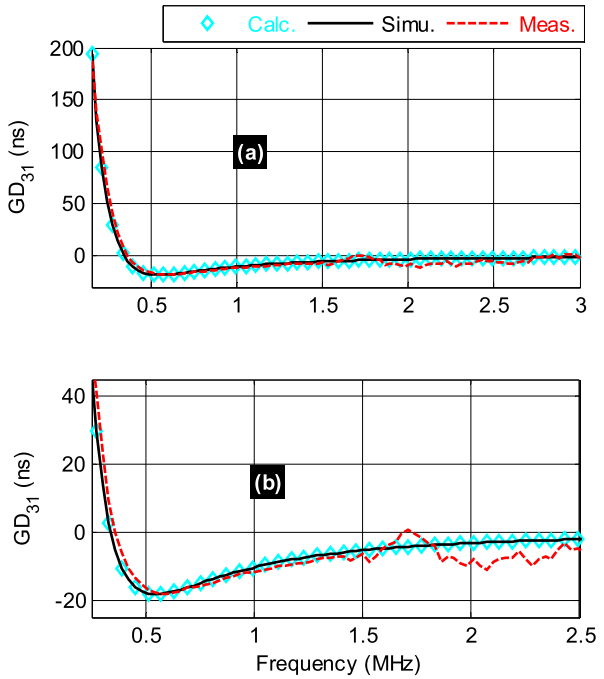

FIGURE 10. Comparisons between simulated, measured and calculated GDs from S_{31} transmission coefficients of the Δ-circuit prototype in (a) wide and (b) narrow band plots.

experimental results is mainly due to the VNA measurement noises. As a conclusion of the plots displayed by Figs. 10, the Δ-circuit implemented as three-port topology of fully capacitive network behaves as a BP NGD function.

5) DISCUSSION ON THE CALCULATED, SIMULATED AND MEASURED NGD PERFORMANCES

The validation of the BP NGD function of the fully capacitive Δ-circuit can be reported with the quantitative specification of:

- NGD center frequency, f_0,
- NGD value, $GD_{31}(f_0)$,
- NGD bandwidth, $\Delta f = f_b - f_a$,
- Attenuation, $S_{31}(f_0)$,
- And reflection coefficient, $S_{11}(f_0)$.

We can summarize the BP NGD specifications defined by Fig. 3 with the comparison of corresponding parameters.

Table 3 summarizes the comparative BP NGD parameters from the simulated, calculated and measured GD plotted in Figs. 10. We can point out that the attenuation is better than -3 dB around the NGD center frequency, $f_0 = 0.55$ MHz. But the reflection losses are slightly less than 7 dB. In the next step of the study, the optimization technique of the four-port NGD circuit will be developed in order to ensure the BP NGD function with respect to the constraints between the reflection and transmission losses.

TABLE 3. Comparison of BP NGD specifications from the GD associated to transmission coefficient S_{31}.

Capacitor	C_{12}	C_{13}	C_{23}
Minimum	95 pF	95 nF	9.5 nF
Maximum	105 pF	105 nF	10.5 nF

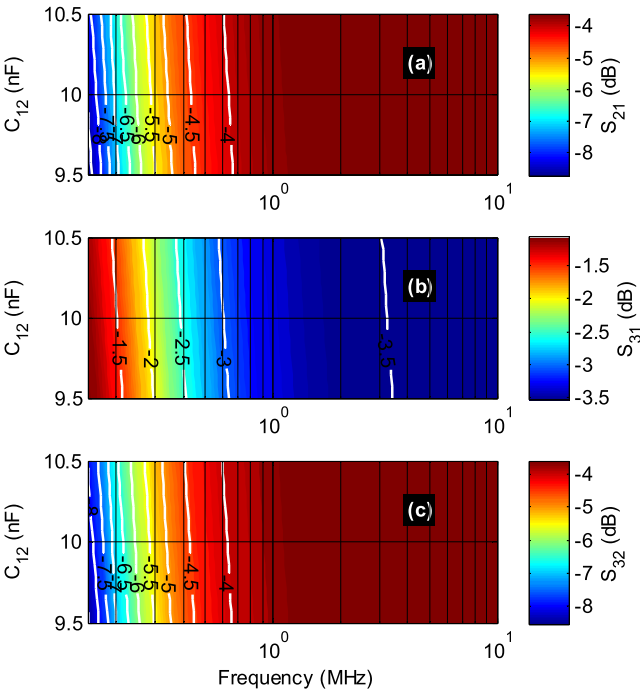

FIGURE 11. Mappings of (a) S_{21}, (b) S_{31} and (c) S_{32} magnitudes versus (f,C_{12}).

C. SENSIVITY ANALYSIS WITH RESPECT TO C_{12}, C_{13} AND C_{23}

The robustness of the BP NGD function with the Δ-circuit is investigated in the present subsection. Doing this, we considered the linear $+/-5\%$ relative variations of each capacitor C_{12}, C_{13} and C_{23}. Table 3 indicates the range of capacitor values.

1) INFLUENCE OF C_{12}

Figs. 11 and Figs. 12 show the semi-logarithmic scale cartographies of the transmission and reflection coefficients of the Δ-circuit versus pair variables (f, C_{12}).

The SA was generated by varying only one of capacitor, C_{12}, under $+/-5\%$ relative variation. The calculation was performed following the range of value indicated by Table 3. The frequency x-axis of Figs. 11 and Figs. 12 is presented in

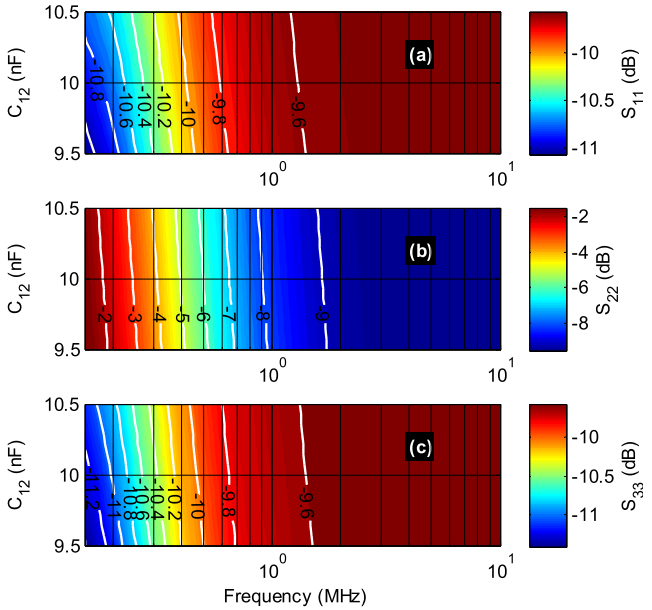

FIGURE 12. Mappings of (a) S_{11}, (b) S_{22} and (c) S_{33} magnitudes versus (f,C_{12}).

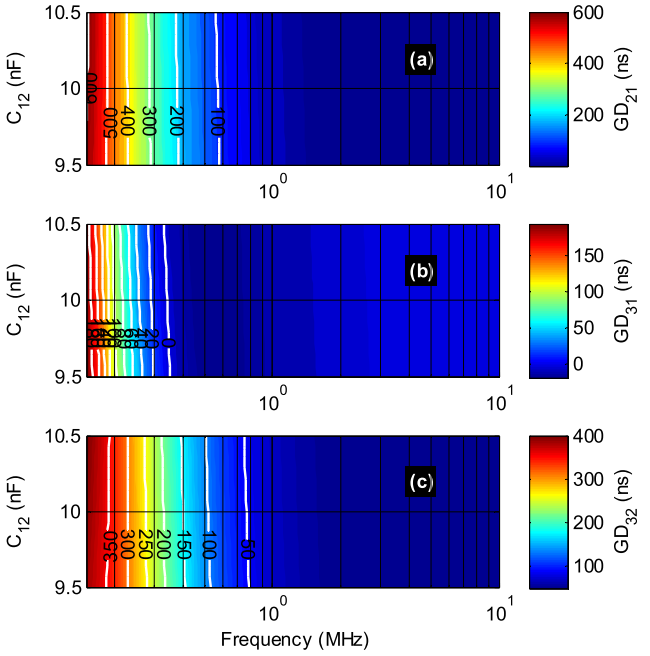

FIGURE 13. Mappings of GD_{21}, GD_{31} and GD_{32} versus (f,C_{12}).

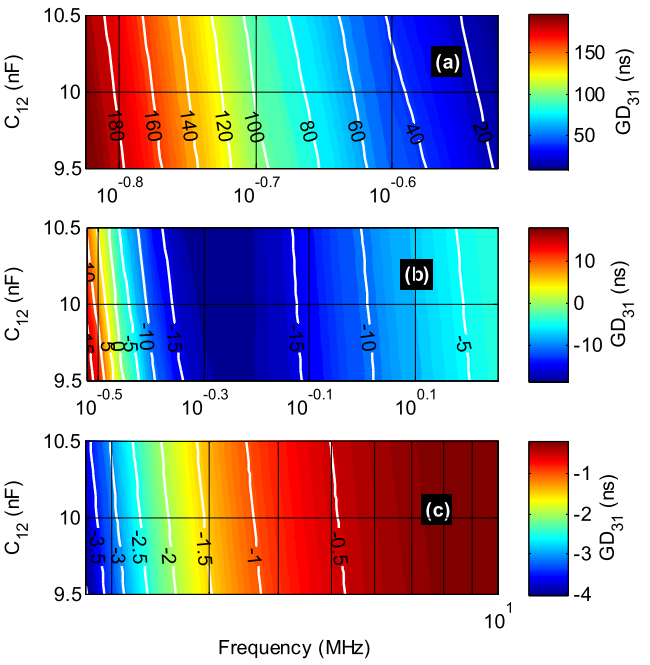

FIGURE 14. Mappings of GD_{31} zoomed in (a) [150 kHz, 300 kHz], (b) [300 kHz, 1.8 MHz] and (c) [1.8 MHz, 10 MHz] versus (f,C_{12}).

logarithmic scale for the better presentation of the responses in the considered range of the frequency. We can emphasize from these cartographies that the magnitudes of the reflection and transmission coefficients of the Δ-circuit decrease when capacitor, C_{12}, increases. It is important to note that with $+/-5\%$ relative variation tolerance, S_{31} remains above -3.5 dB, and, S_{11} and S_{33} are below -9.5 dB.

The more important SA results are introduced by Figs. 13. They concern the GD responses of the Δ-circuit. It can be understood from Fig. 13(a) and Fig. 13(c) that GD_{21} an GD_{32} are always positive in the range of the capacitor variation. To highlight the BP NGD behavior, typical zoomed in plots of three different cartographies of GD_{31} are proposed in Fig. 14(a), Fig. 14(b) and Fig. 14, for the frequency bands:

- $BW_1 = [150\text{ kHz}, 300\text{ kHz}]$,
- $BW_2 = [300\text{ kHz}, 1.8\text{ mHz}]$,
- and $BW_3 = [1.8\text{ mHz}, 10\text{ mHz}]$,

respectively. We can see that the GD is always positive in BW_1. Then, the NGD behavior is observed in BW_2 and BW_3. According to Fig. 14(b) and Fig. 14(c), The NGD center frequency decreases when C_{12} increases.

2) INFLUENCE OF C_{13}

The present SA of C_{13} was performed under the same approach as the previous case of C_{12}. Figs. 15 display the in semi-logarithmic scale cartographies of reflection coefficients, S_{21}, S_{31} and S_{32} versus pair variables (f, C_{13}). The capacitor was linearly varied in the range of values given in Table 3. We can see in Figs. 15, the influence of C_{13} on the transmission coefficients is literally negligible.

Figs. 16 show the cartographies of the reflection coefficients in semi-logarithmic scale. As seen in Fig. 16(b), S_{22} is less sensitive to C_{13}. However, S_{11} and S_{33} change significantly notably in the frequency band below 0.5 MHz. However, we can report that the levels of access matching of port$_1$ and port$_3$ remain below -9.5 dB with $+/-5\%$ relative variation of C_{13}.

Figs. 17 show the mappings of the three GDS of our Δ-circuit versus pair variables (F, C_{13}). It can be understood from Fig. 17(a) and Fig. 17(b) that GD_{21} and GD_{32} are always positive despite the variation of capacitor, C_{13}. However, the BP NGD behavior can be observed in Figs. 18. The same

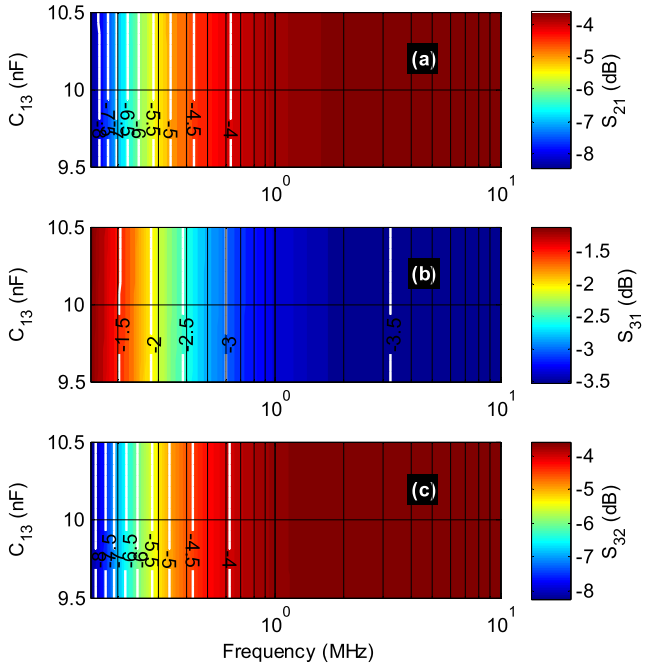

FIGURE 15. Mappings of (a) S_{21}, (b) S_{31} and (c) S_{32} magnitudes versus (f,C_{13}).

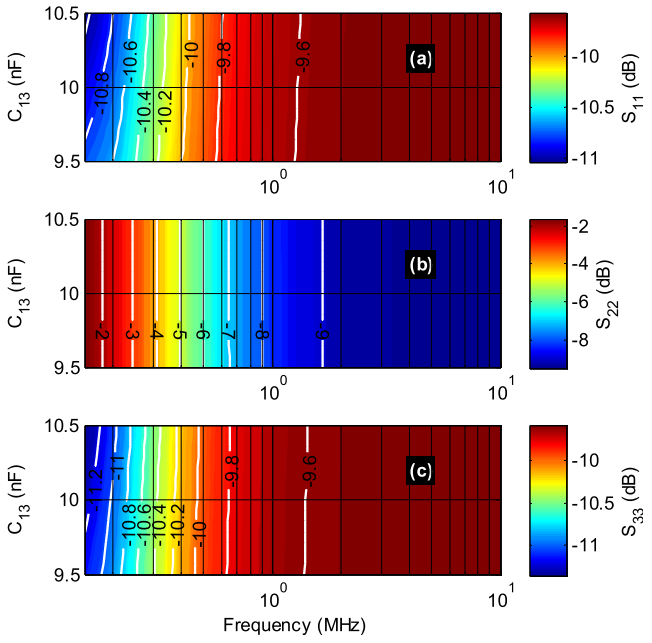

FIGURE 16. Mappings of (a) S_{11}, (b) S_{22} and (c) S_{33} magnitudes versus (f,C_{13}).

as previous case of study the NGD response between port$_1$ and port$_3$ is more obvious in BW_2 and BW_3 as witnessed by cartographies of Fig. 18(b) and Fig. 18(c).

3) INFLUENCE OF C_{23}

The last SA is performed with respect to C_{23}. Figs. 19 represent the in semi-logarithmic scale cartographies of reflection coefficients, S_{21}, S_{31} and S_{32} versus pair variables (f, C_{23}). As aforementioned, C_{23} was linearly varied in the range of

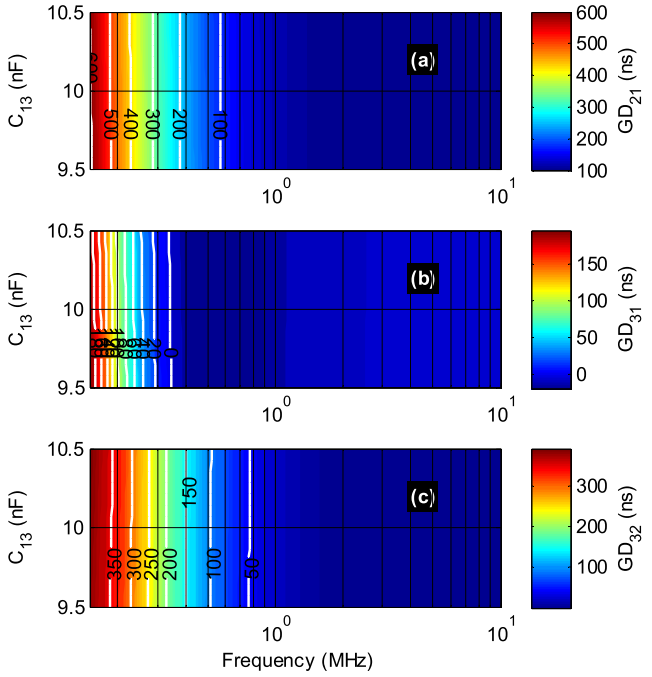

FIGURE 17. Mappings of GD_{21}, GD_{31} and GD_{32} versus (f,C_{13}).

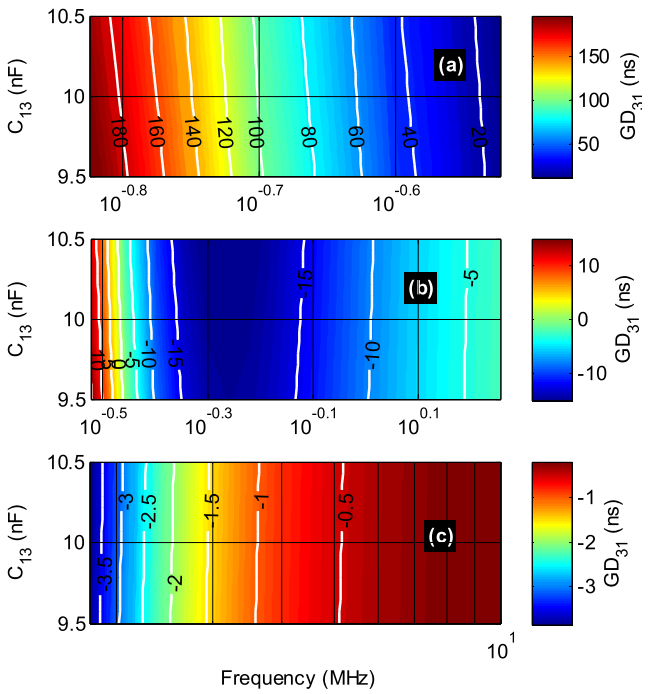

FIGURE 18. Mappings of GD_{31} zoomed in (a) [150 kHz, 300 kHz], (b) [300 kHz, 1.8 MHz] and (c) [1.8 MHz, 10 MHz] versus (f,C_{13}).

values given in Table 3. Similar to previous case, we can see in Figs. 19, the influence of C_{23} on the transmission coefficients is literally negligible. Figs. 20 show the cartographies of the reflection coefficients in semi-logarithmic scale. As seen in Figs. 20, in this case, S_{11}, S_{22} and S_{33} are less sensitive to C_{23}. The reflection coefficients from port$_1$ and

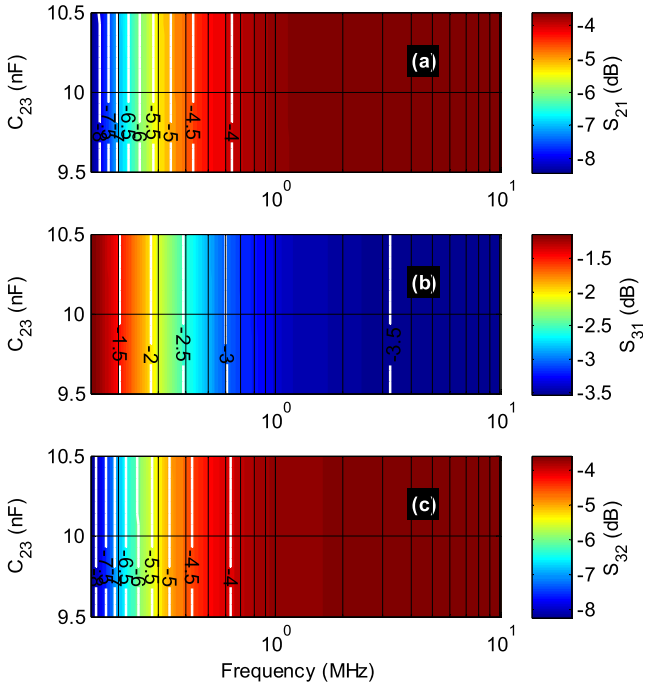

FIGURE 19. Mappings of (a) S_{21}, (b) S_{31} and (c) S_{32} magnitudes versus (f,C_{23}).

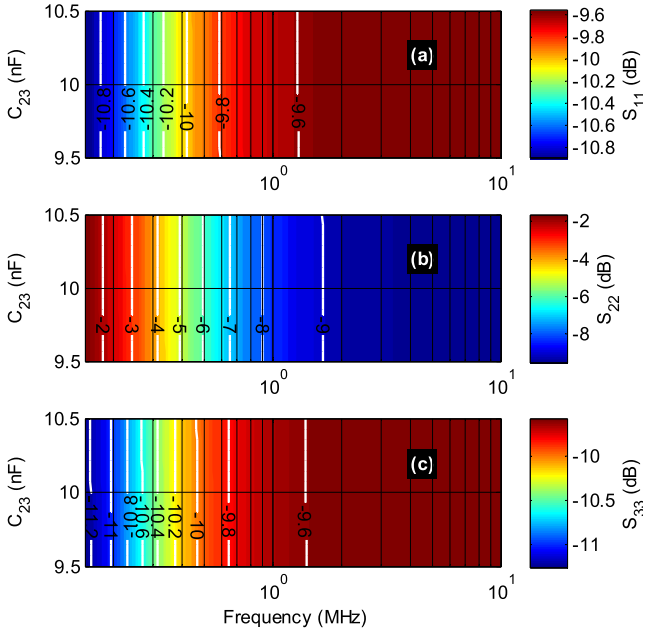

FIGURE 20. Mappings of (a) S_{11}, (b) S_{22} and (c) S_{33} magnitudes versus (f,C_{23}).

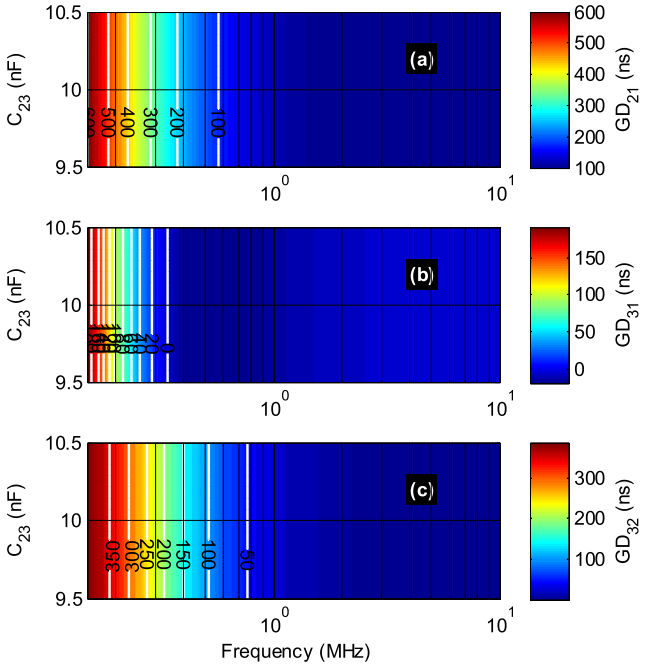

FIGURE 21. Mappings of GD_{21}, GD_{31} and GD_{32} versus (f,C_{23}).

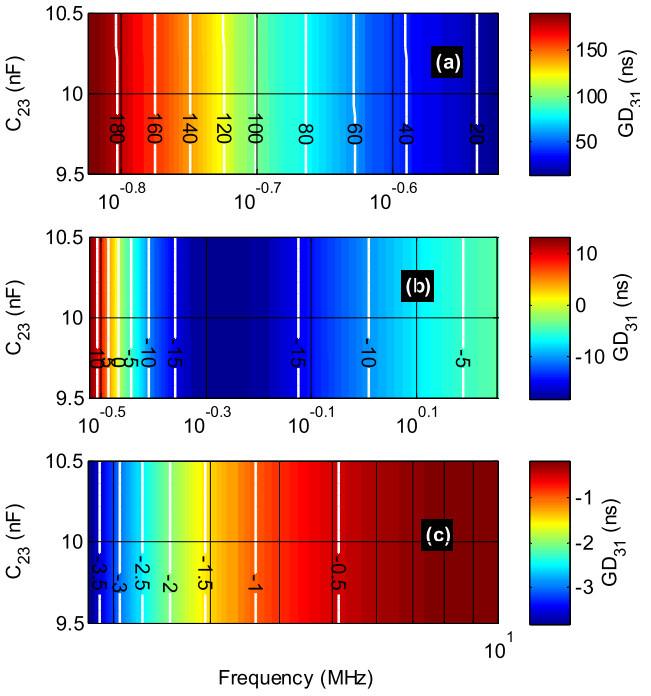

FIGURE 22. Mappings of GD_{31} zoomed in (a) [150 kHz, 300 kHz], (b) [300 kHz, 1.8 MHz] and (c) [1.8 MHz, 10 MHz] versus (f,C_{23}).

port$_3$ remain below -9.5 dB with $+/-5\%$ relative variation of C_{13}.

Figs. 21 show the GD cartographies versus pair variables (F, C_{23}). It can be understood from Figs. 22 that GD_{21} and GD_{32} are always positive despite the variation of capacitor, C_{23}. The BP NGD behavior can be observed in Figs. 22. The same as previous case of study the NGD response between port$_1$ and port$_3$ is more obvious in BW_2 and BW_3 as witnessed by cartographies of Fig. 22(b) and Fig. 22(c). But in this case, the influence of C_{23} on GD_{31} is seemingly negligible.

VI. CONCLUSION

An original circuit theory of BP NGD three-port topology is developed. The Δ-circuit under study is constituted only by fully capacitive network which does not use any resistor and any inductor. The analytical modelling of the typical

three-port lumped circuit is developed from the admittance matrix. The S-parameter analytical model is determined from the Y-to-S matrix transform. The methodology of the BP NGD analysis is described by expressing the appropriated characteristics of the Δ-topology.

The design feasibility of the original Δ-topology is performed with a lumped circuit prototype with commercial components. The transmission and reflection coefficients from analytical calculation, commercial tool-based simulation and measurement are compared. The measurement was carried out in three-port configuration by using a VNA. The modelling validation is verified with the plots of the tested Δ-circuit reflection and transmission coefficients. Furthermore, the BP NGD analysis is validated by the GD response between port 1 and port 3 of the Δ-circuit prototype.

REFERENCES

[1] S. Chu and S. Wong, "Linear pulse propagation in an absorbing medium," *Phys. Rev. Lett.*, vol. 48, no. 11, pp. 738–741, Mar. 1982.

[2] B. Segard and B. Macke, "Observation of negative velocity pulse propagation," *Phys. Lett. A*, vol. 109, no. 5, pp. 213–216, May 1985.

[3] B. Macke and B. Ségard, "Propagation of light-pulses at a negative group-velocity," *Eur. Phys. J. D, At., Mol. Opt. Phys.*, vol. 23, no. 1, pp. 125–141, Apr. 2003.

[4] J. N. Munday and W. M. Robertson, "Observation of negative group delays within a coaxial photonic crystal using an impulse response method," *Opt. Commun.*, vol. 273, no. 1, pp. 32–36, May 2007.

[5] H. Cao, A. Dogariu, and L. J. Wang, "Negative group delay and pulse compression in superluminal pulse propagation," *IEEE J. Sel. Topics Quantum Electron.*, vol. 9, no. 1, pp. 52–58, Jan. 2003.

[6] B. Macke, B. Ségard, and F. Wielonsky, "Optimal superluminal systems," *Phys. Rev. E, Stat. Phys. Plasmas Fluids Relat. Interdiscip. Top.*, vol. 72, no. 3, Sep. 2005, Art. no. 035601(R).

[7] B. Macke and B. Ségard, "Two-pulse interference and superluminality," *Opt. Commun.*, vol. 281, no. 1, pp. 12–17, Jan. 2008.

[8] H. Mao, L. Ye, and L.-G. Wang, "High fidelity of electric pulses in normal and anomalous cascaded electronic circuit systems," *Results Phys.*, vol. 13, Jun. 2019, Art. no. 102348.

[9] J. N. Munday and R. H. Henderson, "Superluminal time advance of a complex audio signal," *Appl. Phys. Lett.*, vol. 85, no. 3, pp. 503–505, Jul. 2004.

[10] M. W. Mitchell and R. Y. Chiao, "Negative group delay and 'fronts' in a causal system: An experiment with very low frequency bandpass amplifiers," *Phys. Lett. A*, vol. 230, nos. 3–4, pp. 133–138, Jun. 1997.

[11] M. W. Mitchell and R. Y. Chiao, "Causality and negative group delays in a simple bandpass amplifier," *Amer. J. Phys.*, vol. 66, no. 1, pp. 14–19, Jan. 1998.

[12] M. Kitano, T. Nakanishi, and K. Sugiyama, "Negative group delay and superluminal propagation: An electronic circuit approach," *IEEE J. Sel. Topics Quantum Electron.*, vol. 9, no. 1, pp. 43–51, Jan. 2003.

[13] G. V. Eleftheriades, O. Siddiqui, and A. K. Iyer, "Transmission line models for negative refractive index media and associated implementations without excess resonators," *IEEE Microw. Wireless Compon. Lett.*, vol. 13, no. 2, pp. 51–53, Feb. 2003.

[14] O. F. Siddiqui, M. Mojahedi, and G. V. Eleftheriades, "Periodically loaded transmission line with effective negative refractive index and negative group velocity," *IEEE Trans. Antennas Propag.*, vol. 51, no. 10, pp. 2619–2625, Oct. 2003.

[15] O. F. Siddiqui, S. J. Erickson, G. V. Eleftheriades, and M. Mojahedi, "Time-domain measurement of negative-index transmission-line metamaterials," *IEEE Trans. Microw. Theory Techn.*, vol. 52, no. 5, pp. 1449–1453, May 2004.

[16] T. Kokkinos, C. D. Sarris, and G. V. Eleftheriades, "Periodic finite-difference time-domain analysis of loaded transmission-line negative-refractive-index metamaterials," *IEEE Trans. Microw. Theory Techn.*, vol. 53, no. 4, pp. 1488–1495, Apr. 2005.

[17] L. Markley and G. V. Eleftheriades, "Quad-band negative-refractive-index transmission-line unit cell with reduced group delay," *Electron. Lett.*, vol. 46, no. 17, pp. 1206–1208, Aug. 2010.

[18] G. Monti and L. Tarricone, "Negative group velocity in a split ring resonator-coupled microstrip line," *Prog. Electromagn. Res.*, vol. 94, pp. 33–47, 2009.

[19] T. Nesimoglu and C. Sabah, "A tunable metamaterial resonator using varactor diodes to facilitate the design of reconfigurable microwave circuits," *IEEE Trans. Circuits Syst. II, Exp. Briefs*, vol. 63, no. 1, pp. 89–93, Jan. 2016.

[20] J. J. Barroso, J. E. B. Oliveira, O. L. Coutinho, and U. C. Hasar, "Negative group velocity in resistive lossy left-handed transmission lines," *IET Microw., Antennas Propag.*, vol. 10, no. 7, May 2016, pp. 808–815.

[21] H. Choi, Y. Jeong, C. D. Kim, and J. S. Kenney, "Bandwidth enhancement of an analog feedback amplifier by employing a negative group delay circuit," *Prog. Electromagn. Res.*, vol. 105, pp. 253–272, 2010.

[22] B. Ravelo, "Distributed NGD active circuit for RF-microwave communication," *AEU-Int. J. Electron. Commun.*, vol. 68, no. 4, pp. 282–290, Apr. 2014.

[23] A. Mortazawi and W. Alomar, "Negative group delay circuit," U.S. Patent Appl. US 2016 0 093 958, Mar. 2016.

[24] M. Zhu and C.-T.-M. Wu, "Reconfigurable series feed network for squint-free antenna beamforming using distributed amplifier-based negative group delay circuit," in *Proc. 49th Eur. Microw. Conf. (EuMC)*, Paris, France, Oct. 2019, pp. 256–259.

[25] B. Ravelo, S. Lalléchère, A. Thakur, A. Saini, and P. Thakur, "Theory and circuit modeling of baseband and modulated signal delay compensations with low- and band-pass NGD effects," *AEU-Int. J. Electron. Commun.*, vol. 70, no. 9, pp. 1122–1127, Sep. 2016.

[26] T. Shao, Z. Wang, S. Fang, H. Liu, and Z. N. Chen, "A group-delay-compensation admittance inverter for full-passband self-equalization of linear-phase band-pass filter," *Int. J. Electron. Commun.*, vol. 123, Aug. 2020, Art. no. 153297.

[27] T. Zhang, C.-T. M. Wu, and R. Xu, "High Q series negative capacitor using negative group delay circuit based on a stepped-impedance distributed amplifier," *IEICE Electron. Exp.*, vol. 14, no. 7, pp. 1–6, Apr. 2017.

[28] K.-P. Ahn, R. Ishikawa, A. Saitou, and K. Honjo, "Synthesis for negative group delay circuits using distributed and second-order RC circuit configurations," *IEICE Trans. Electron.*, vol. E92-C, no. 9, pp. 1176–1181, 2009.

[29] G. Chaudhary and Y. Jeong, "Negative group delay phenomenon analysis using finite unloaded quality factor resonators," *Prog. Electromagn. Res.*, vol. 156, pp. 55–62, Jun. 2016.

[30] Z. Wang, Y. Cao, T. Shao, S. Fang, and Y. Liu, "A negative group delay microwave circuit based on signal interference techniques," *IEEE Microw. Wireless Compon. Lett.*, vol. 28, no. 4, pp. 290–292, Apr. 2018.

[31] G. Chaudhary and Y. Jeong, "Transmission-type negative group delay networks using coupled line doublet structure," *IET Microw., Antennas Propag.*, vol. 9, no. 8, pp. 748–754, Jun. 2015.

[32] B. Ravelo, "Theory of coupled line coupler-based negative group delay microwave circuit," *IEEE Trans. Microw. Theory Techn.*, vol. 64, no. 11, pp. 3604–3611, Nov. 2016.

[33] G. Chaudhary and Y. Jeong, "Tunable center frequency negative group delay filter using coupling matrix approach," *IEEE Microw. Wireless Compon. Lett.*, vol. 27, no. 1, pp. 37–39, Jan. 2017.

[34] R. Das, Q. Zhang, and H. Liu, "Lossy coupling matrix synthesis approach for the realization of negative group delay response," *IEEE Access*, vol. 6, pp. 1916–1926, 2018.

[35] T. Shao, Z. Wang, S. Fang, H. Liu, and S. Fu, "A compact transmission-line self-matched negative group delay microwave circuit," *IEEE Access*, vol. 5, pp. 22836–22843, 2017.

[36] G. Liu and J. Xu, "Compact transmission-type negative group delay circuit with low attenuation," *Electron. Lett.*, vol. 53, no. 7, pp. 476–478, Mar. 2017.

[37] T. Shao, S. Fang, Z. Wang, and H. Liu, "A compact dual-band negative group delay microwave circuit," *Radioengineering*, vol. 27, no. 4, pp. 1070–1076, Dec. 2018.

[38] S. Lucyszyn and I. D. Robertson, "Analog reflection topology building blocks for adaptive microwave signal processing applications," *IEEE Trans. Microw. Theory Techn.*, vol. 43, no. 3, pp. 601–611, Mar. 1995.

[39] C. D. Broomfield and J. K. A. Everard, "Broadband negative group delay networks for compensation of microwave oscillators and filters," *Electron. Lett.*, vol. 36, no. 23, pp. 1931–1933, Nov. 2000.

[40] M. Kandic and G. E. Bridges, "Asymptotic limits of negative group delay in active resonator-based distributed circuits," *IEEE Trans. Circuits Syst. I, Reg. Papers*, vol. 58, no. 8, pp. 1727–1735, Aug. 2011.
[41] C.-T.-M. Wu and T. Itoh, "Maximally flat negative group-delay circuit: A microwave transversal filter approach," *IEEE Trans. Microw. Theory Techn.*, vol. 62, no. 6, pp. 1330–1342, Jun. 2014.
[42] F. Wan, N. Li, B. Ravelo, J. Ge, and B. Li, "Time-domain experimentation of NGD ActiveRC-network cell," *IEEE Trans. Circuits Syst. II, Exp. Briefs*, vol. 66, no. 4, pp. 562–566, Apr. 2019.
[43] Y. Meng, Z. Wang, S. Fang, T. Shao, and H. Liu, "A broadband switchless bi-directional amplifier with negative-group-delay matching circuits," *Electronics*, vol. 7, no. 9, pp. 1–11, Aug. 2018.
[44] B. Ravelo, "Similitude between the NGD function and filter gain behaviours," *Int. J. Circ. Theor. Appl.*, vol. 42, no. 10, pp. 1016–1032, Oct. 2014.
[45] B. Ravelo, "First-order low-pass negative group delay passive topology," *Electron. Lett.*, vol. 52, no. 2, pp. 124–126, Jan. 2016.
[46] B. Ravelo, "High-pass negative group delay RC-network impedance," *IEEE Trans. Circuits Syst. II, Exp. Briefs*, vol. 64, no. 9, pp. 1052–1056, Sep. 2017.
[47] B. Ravelo, S. Ngoho, G. Fontgalland, L. Rajaoarisoa, W. Rahajandraibe, R. Vauché, Z. Xu, F. Wan, J. Ge, and S. Lalléchère, "Original theory of NGD low pass-high pass composite function for designing inductorless BP NGD lumped circuit," *IEEE Access*, vol. 8, pp. 192951–192964, 2020.

FAYU WAN (Member, IEEE) received the Ph.D. degree in electronic engineering from the University of Rouen, Rouen, France, in 2011. From 2011 to 2013, he was a Postdoctoral Fellow with the Electromagnetic Compatibility Laboratory, Missouri University of Science and Technology, Rolla. He is currently a Full Professor with the Nanjing University of Information Science and Technology, Nanjing, China. His current research interests include negative group delay circuits, electrostatic discharge, electromagnetic compatibility, and advanced RF measurement.

YANG LIU was born in Dalian, Liaoning, China, in 1982. He received the B.Sc. degree in technics of control, measurement and instrumentation from the Dalian University of Technology, Dalian, in July 2004, and the B.Sc. and M.Sc. degrees in electronic engineering from the University of Pierre and Marie Curie (UPMC), Paris, France, in July 2007 and July 2009, respectively, and the Ph.D. degree from the IRSEEM/ESIGELEC, University of Rouen, France, in October 2012.

JAMEL NEBHEN (Member, IEEE) received the M.Sc. degree from the National Engineering School of Sfax, Tunisia, in 2007, and the Ph.D. degree from Aix-Marseille University, France, in 2012, both in microelectronics. From 2012 to 2018, he worked as a Postdoctoral Researcher in France at the LIRMM-Laboratory Montpellier, the IM2NP-Laboratory Marseille, the ISEP Paris, LE2I-Laboratory Dijon, the Laboratory-Sticc Telecom Bretagne Brest, and the IEMN-Laboratory Lille. Since 2019, he has been with Prince Sattam Bin Abdulaziz University, Alkharj, Saudi Arabia, as an Assistant Professor. His research interests include mainly in the design of analog and RF integrated circuits, the IoT, biomedical circuit, and sensors instrumentation.

ZHIFEI XU (Member, IEEE) received the Ph.D. degree from the University of Rouen, France, in 2019. He is currently doing the postdoctoral research at the EMC-Laboratory, Missouri S&T, USA. He developed Kron-Branin model for multilayer PCB modeling applications. He published book and extensive publications with related expertise in high-speed signal/power integrity and EMC design. His current publications are focusing on the advanced/optimized algorithms/tools with respect to the functions for signal/power and EMC analysis for high-speed PCB design. His research interests include signal integrity, power integrity, and EMC analysis with different models on multilayer PCBs.

GEORGE CHAN (Senior Member, IEEE) received the B.Eng. degree (Hons.) in electronic and communication engineering from the City University of Hong Kong, and the M.Sc. degree in electronic and information engineering from The Hong Kong Polytechnic University.

He is currently a Senior Product Safety Engineer with ASM Pacific Technology Ltd. He has coauthored several technical publications in international journals and conference proceedings. His research interests include electromagnetic safety, EMC measurement, and EMC management. He is a member of the IEEE EMC Society TC1 on EMC Management. He is also a member of the IEEE International Committee for Electromagnetic safety (ICES) Standards Coordinating Committee (SCC39) and a TC95 Sub-Committee Member. He is an International Electrotechnical Commission (IEC) Expert and a Committee Member of IEC TC106/PT63184 on method for the assessment of electric, magnetic, and electromagnetic fields associated with human exposure.

SÉBASTIEN LALLÉCHÈRE (Member, IEEE) was born in Nevers, France, in 1979. He received the M.Sc. degree in computational modeling from Polytech Clermont-Ferrand, France, in 2002, and the Ph.D. degree in electronics/electromagnetism from Universite Blaise Pascal, Clermont-Ferrand, France, in 2006.

In 2007, he served as a Research Engineer with LASMEA, Clermont-Ferrand, France, focusing on intensive computational methods for electromagnetics. He is currently an Associate Professor with the Institut Pascal and Universite Clermont Auvergne, Clermont-Ferrand. His research interest includes the fields of electromagnetic compatibility, including antennas and propagation, complex and reverberating electromagnetic environments, electromagnetic coupling, computational electromagnetics, stochastic modeling, and sensitivity analysis in electrical engineering.

RÉMY VAUCHE (Member, IEEE) received the M.Eng. degree in microelectronics and telecommunication from Polytech' Marseille, Marseille, France, in 2008, the M.S. degree in microelectronics and nanoelectronics from Aix-Marseille University, Marseille, in 2008, and the Ph.D. degree in microelectronics from the University of Provence, Marseille, in 2011.

From 2011 to 2014, he was a Lecturer and a Researcher with the ISEN French Engineering School, Toulon, France. Since 2014, he has been an Associate Professor with Aix-Marseille University. He is currently a member of the Provence Nanosciences Microelectronics and Materials Laboratory, Integrated Circuits Design Team, Marseille. His current research interests include mainly the design of integrated circuits and systems for ultra-wideband impulse radio, human body communications, and home-care applications.

WENCESLAS RAHAJANDRAIBE (Member, IEEE) is currently a Full Professor with the University of Aix-Marseille. He received the B.Sc. degree in electrical engineering from Nice Sophia-Antipolis University, France, in 1996, and the M.Sc. degree (Hons.) in electrical engineering from the Department of Science, University of Montpellier, France, in 1998. In 1998, he was with the Informatics, Robotics and Microelectronics Laboratory of Montpellier (LIRMM), Department of Microelectronics, and the Ph.D. degree in microelectronics form the University of Montpellier. In 2003, he was with the Materials, Microelectronics and Nanoscience Laboratory of Provence (IM2NP), Department of Microelectronic, Marseille, France, as an Associate Professor. Since 2014, he has been a Professor with Aix Marseille University, where he heads the IM2NP Laboratory, Integrated Circuit Design Group. He directed and co-supervised 18 Ph.D. and 15 Master students. He is regularly involved to participate and to lead national and international research projects (ANR, H2020, FP7 KIC-InnoEnergy…). He has authored or coauthored 11 patents and more than 150 papers published in refereed journals and conferences. His research interests include AMS and RF circuit design from transistor to architectural level. His current research interests include ultralow power circuit design for smart sensor interface and embedded electronic in bio-electronic and e-health applications, wireless systems, design technique, and architecture for multi-standard transceiver. He is an Expert for the ANR, the French Agency for Research. He has served on program committees of IEEE NEWCAS and ICECS. He has been and is a Reviewer of contributions submitted to several IEEE conferences and journals, such as ISCAS, NEWCAS, MWSCAS, ESSCIRC, ESSDERC, RFIC, IEEE TRANSACTIONS ON CIRCUITS AND SYSTEMS I and IEEE TRANSACTIONS ON CIRCUITS AND SYSTEMS II, and *Electronics Letters* (IET).

BLAISE RAVELO (Member, IEEE) was a Research Director of 11 Ph.D. students (eight defended), postdoctorates, research engineers, and master internships. He is currently a Full Professor with the Nanjing University of Information Science and Technology (NUIST), Nanjing, China. He is a Lecturer on circuit and system theory, and STEM (science, technology, engineering, and maths) and applied physics. He is also a Pioneer of the negative group delay (NGD) concept about $t<0$ signal travelling physical space. This extraordinary concept is potentially useful for anticipating and prediction all kind of information. With USA, Chinese, Indian, European, and African partners, he is actively involved and contributes on several international research projects, such as ANR, FUI, FP7, INTERREG, H2020, Euripides^2, Eurostars, and so on. He coauthored more than 340 scientific research papers in new technologies published in international conferences and journals. His research interests include multiphysics and electronics engineering. He has been a member of the Scientific Technical Committee of Advanced Electromagnetic Symposium (AES), since 2013. He is a member of research groups, namely IEEE, URSI, GDR Ondes, Radio Society. He is a member of the IET *Electronics Letters* Editorial Board, as a Circuit and System Subject Editor. He regularly invited to review papers submitted for publication to international journals IEEE TRANSACTIONS ON MICROWAVE THEORY AND TECHNIQUES, IEEE TRANSACTIONS ON CIRCUITS AND SYSTEMS, IEEE TRANSACTIONS ON ELECTROMAGNETIC COMPATIBILITY, IEEE TRANSACTIONS ON INDUSTRIAL ELECTRONICS, IEEE ACCESS, IET *CDS*, IET *MAP*, and so on), and books (Wiley, Intech Science, and so on). He has Google scholar h-index(2021)=22 and i10-index(2021)=60.